Accepted for presentation at the 11th European Wave and Tidal Energy Conference (EWTEC 2015) 6-11 September 2015, Nantes, France.

Final Draft (25th June 2015)

Numerical Validation of the Two-Scale Actuator Disc Theory for Marine Turbine Arrays

Edgar Perez-Campos*, Takafumi Nishino[1]

Centre for Offshore Renewable Energy Engineering, Cranfield University
Cranfield, Bedfordshire MK43 0AL, UK

[1]t.nishino@cranfield.ac.uk

***Abstract*—The challenge in the hydrodynamic modelling of tidal and marine turbine farms is to take into account the interaction of flow events across a wide range of scales, such as the blade scale, turbine scale, array scale and regional scale. Whilst the interaction of the blade and turbine scales can be studied using the classical Blade-Element-Momentum (BEM) theory, no basic theory was available until recently to describe the interaction of the turbine and larger scales. The two-scale actuator disc theory (ADT), first proposed in 2012 by Nishino and Willden, explains the interaction of the turbine and array scales at a fundamental level; however, its validity or applicability to real problems has only partially been confirmed. Hence in this study we perform 3D RANS simulations of single and double rows of porous discs (8 discs for each row) in the middle of a shallow open channel with a vertically sheared flow. The simulation results are shown to agree qualitatively with the two-scale ADT and importantly, the optimal intra-disc spacing predicted by the simulations (to maximise the total power) agrees well with the theory, for both single- and double-row cases.**

***Keywords*—Tidal stream energy, Ocean current energy, Multi-scale modelling, Hydrodynamics, Optimal turbine array**

I. Introduction

Tidal currents are one of the most promising sources of renewable energy especially for countries with suitable marine conditions. The maximum power extracted from a fluid flow, independently of the device design, can be assessed using the Linear Momentum Actuator Disk Theory (LMADT) [1]. This theory was derived originally to predict the performance of wind turbines and rotorcraft applications; however, the theory was then extended for tidal applications, for which the power extracted is strongly influenced by the blockage of the tidal channel [2]–[4]. Most importantly, the maximum power of a turbine placed in a channel is proportional to $(1 - B)^{-2}$, where B is the channel's cross-sectional blockage ratio.

Following the above-mentioned studies on the maximum power of a tidal turbine in a channel, Nishino & Willden [5] carried out a further theoretical investigation focusing on the efficiency of a lateral array of turbines partially blocking a wide water channel. This study introduced the idea of scale separation between the flow around each device and that around the whole array. Although this extended actuator disc theory (namely the two-scale Actuator Disc Theory) is still a simple one-dimensional quasi-inviscid theory neglecting the effect of seabed friction and the resulting vertical shear of the flow, it has been shown to be useful to understand the basic effects of local and global blockages on the performance of a lateral array of turbines [5], [6]. A more recent explanation of the physical meaning of the local and global blockage effects has been given by Nishino and Draper [7].

One of the challenges in the hydrodynamic modelling of tidal turbine arrays is how to model the interaction of flow events across a wide range of scales, such as the blade scale, turbine scale, array scale and regional scale [8]. Similarly to the classical Blade-Element-Momentum (BEM) theory being very useful to understand the interaction of blade and turbine scales, the two-scale ADT is expected to become an important basis to understand the interaction of turbine and array scales. However, since the theory is based on many assumptions, it is crucial to assess its validity or applicability to real problems and, if necessary, make some corrections (like we often make tip/hub-loss corrections to the BEM theory, for example).

In this study we perform 3D Reynolds-averaged Navier-Stokes (RANS) simulations of single and double lateral rows of turbines (modelled as actuator discs) placed in the middle of a wide water channel. The results are then compared with the two-scale ADT to assess its validity. Specifically, we aim to assess whether the theory is still approximately valid in a practical situation where (i) the flow is vertically sheared due to the effect of the seabed and (ii) not only single but also double rows of turbines are deployed. The single- and multi-row versions of the two-scale ADT are briefly described first in Section II, followed by the details of the RANS simulations in Section III. Results are presented in Section IV and finally conclusions are given in Section V.

II. Two-Scale Actuator Disc Theory

We first describe briefly the original two-scale ADT for a single row of a number of turbines placed in the middle of a wide water channel. We then describe a possible extension of this theory to double (and more) rows of turbines.

A. Single Row

The two-scale ADT was proposed by Nishino and Willden [5] originally for a single lateral row of turbines. The basic assumption is that the number of turbines arrayed is large enough to ensure a clear "scale separation" between the flow around each turbine and that around the whole array. For the

* Current affiliation: London Offshore Engineering Department, ABS Europe Ltd., London E1 7HR, UK

case of a single row of turbines, this assumption seems valid (at least approximately) when the number of turbines arrayed is of the order of 10 [6].

For such a long single row of turbines, we can consider the flow around each turbine (i.e. device-scale flow) and the flow around the whole array (i.e. array-scale flow) separately. The only issue here is that for the device-scale flow, the upstream flow speed is not known *a priori* (because it depends on how much the entire channel flow bypasses the whole array). By applying the single-scale blockage effect analysis of Garrett and Cummins [2] to each of the device-scale and array-scale flow problems, we can obtain the following relationships (see [5] and [3] for further details):

$$(1-a_L)=\frac{1+\gamma_L}{(1+B_L)+\sqrt{(1-B_L)^2+B_L(1-1/\gamma_L)^2}} \tag{1}$$

$$(1-a_A)=\frac{1+\gamma_A}{(1+B_A)+\sqrt{(1-B_A)^2+B_A(1-1/\gamma_A)^2}} \tag{2}$$

where a_L and a_A are the axial induction factors for the device- and array-scale problems, γ_L and γ_A are the ratios of the near-wake velocity to the upstream velocity, again for the device- and array-scale problems, and B_L and B_A are the local and array blockage ratios, i.e. the blockage ratios for the device- and array-scale problems. Also, we can obtain the following:

$$C_{TL}=(1-\gamma_L)\left[\frac{(1+\gamma_L)-2B_L(1-a_L)}{(1-B_L(1-a_L)/\gamma_L)^2}\right] \tag{3}$$

$$C_{TA}=(1-\gamma_A)\left[\frac{(1+\gamma_A)-2B_A(1-a_A)}{(1-B_A(1-a_A)/\gamma_A)^2}\right] \tag{4}$$

where C_{TL} and C_{TA} are the thrust coefficients for the device- and array-scale problems. In order to solve the entire problem (or to obtain the relationship between a_L and a_A) we need to couple the device- and array-scale problems in such a way that (i) the mass flow through the entire array is the same between the two problems, and (ii) the total thrust acting on the entire array is the same between the two problems. As described in [5] the coupling condition to be satisfied is therefore

$$C_{TA}=(1-a_A)^2 B_L C_{TL} \tag{5}$$

A common procedure to solve this two-scale problem (for a given set of B_L and B_A) is as follows:

1. Solve the device-scale problem, i.e. obtain a_L and C_{TL} as a function of γ_L, using Eqs (1) and (3).
2. Solve the array-scale problem, i.e. obtain a_A and C_{TA} as a function of γ_A, using Eqs (2) and (4).
3. Find (numerically) the value of a_A that satisfies the coupling condition, Eq. (5), for a given a_L (or C_{TL}).
4. Finally, the (global) thrust and power coefficients of the turbines can be calculated from the following Eqs (6) and (7), respectively, for a given a_L (or C_{TL}):

$$C_{TG}=(1-a_A)^2 C_{TL} \tag{6}$$

$$C_{PG}=(1-a_G)C_{TG}=(1-a_A)^3(1-a_L)C_{TL} \tag{7}$$

where a_G is the (global) axial induction factor [5].

B. Double Rows

The above two-scale ADT can be extended to double (and more) rows of turbines if we assume that: (i) the streamwise spacing between each row, s_R, is large enough to neglect the device-scale wake interaction (i.e. s_R is large enough for the wake of each turbine to be fully mixed before being affected by the turbines downstream); and (ii) the streamwise extent of the region in which we observe the device-scale flow events (approximately $n_R s_R$, where n_R is the number of rows) is still much smaller than the scale for the array-scale (or horizontal) flow expansion and mixing (so that the n_R rows of turbines can still be modelled as a single power-extracting fence from the array-scale point of view) [9].

It should be noted that these assumptions become more and more difficult to be satisfied as n_R increases. The number of turbines (arrayed within each row) required for the theory to be valid is expected to be n_R times more than that required for the single row case. Nevertheless, for such long/wide lateral rows of turbines satisfying the above two assumptions, we can apply the two-scale ADT in a very similar way to the single row case. The only difference is the coupling condition to be satisfied between the device- and array-scale problems (Eq. (5)), which needs to be replaced by the following:

$$C_{TA}=n_R(1-a_A)^2 B_L C_{TL} \tag{8}$$

Note that $n_R = 2$ for the double row case to be discussed later in this paper.

Another application of the two-scale ADT to double rows of turbines has recently been proposed by Draper and Nishino [10]. In their study, two rows of turbines are modelled (from the array-scale point of view) as two power-extracting fences rather than as a single power-extracting fence, with assuming that the downstream fence is located at the end of the "near wake" of the upstream fence (approximately one to two fence-widths downstream of the upstream fence). This approach is expected to be more appropriate when the number of turbines (arrayed within each row) is not large enough. However, in the present study we use the former approach using Eq. (8) for simplicity. Although not shown here, these two approaches tend to yield similar results unless the thrust acting on each fence is very large.

III. RANS Simulations

A. Flow Configurations

As mentioned earlier, in this study we perform 3D RANS simulations of single and double rows of 8 turbines (modelled as porous discs) in a wide water channel. The turbines have a diameter, d, of 20m and are arrayed at the centre of a wide rectangular channel. The streamwise length of the channel is $200d$ (4000m), its height h is $2d$ (40m) and its width w is $40d$ (800m). The lateral spacing between each turbine, s, varies from $0.25d$ to $4d$. For the double row cases, the streamwise spacing between the rows is fixed at $10d$ (200m). Cartesian coordinates (x, y, z) are employed to represent the spanwise, vertical and streamwise directions, respectively.

It should be noted that a very long channel (computational domain) has been used in this study to ensure that the sheared

TABLE I
SUMMARY OF FLOW CONFIGURATIONS FOR RANS SIMULATIONS

Number of rows (n_R)	s/d	Resistance coefficient (K)	B_L	B_A	B_G
1	0.25	2.0, 2.5, 3.0, 3.5, 4.0, 4.5, 5.0, 5.5	0.3142	0.25	0.0785
1	0.5	2.0, 2.5, 3.0, 3.5, 4.0, 4.5, 5.0, 5.5	0.2618	0.3	0.0785
1	1	2.0, 2.5, 3.0, 3.5, 4.0, 4.5, 5.0, 5.5	0.1963	0.4	0.0785
1	4	2.0, 2.5, 3.0, 3.5, 4.0, 4.5, 5.0, 5.5	0.0785	1	0.0785
2	0.25	1.0, 1.5, 2.0, 2.5, 3.0, 3.5, 4.0, 4.5, 5.0, 5.5, 6.0	0.3142	0.25	0.0785
2	0.5	1.0, 1.5, 2.0, 2.5, 3.0, 3.5, 4.0, 4.5, 5.0, 5.5, 6.0	0.2618	0.3	0.0785
2	1	1.0, 1.5, 2.0, 2.5, 3.0, 3.5, 4.0, 4.5, 5.0, 5.5, 6.0	0.1963	0.4	0.0785
2	4	1.0, 1.5, 2.0, 2.5, 3.0, 3.5, 4.0, 4.5, 5.0, 5.5, 6.0	0.0785	1	0.0785

flow profile develops sufficiently before the flow reaches the turbines at the centre of the channel. Table 1 summarizes the flow configurations simulated. Note that the global blockage ratio B_G (= $B_L B_A$) is identical for all cases. The channel inlet velocity, u, is fixed at 2m/s, resulting in the Reynolds number (based on the channel height) Re = $\rho uh/\mu = 8\times10^7$ (where ρ = 1000kg/m^3 and μ = 0.001kg/m-s).

B. Mathematical models

The governing equations of the flow to be solved are 3D incompressible RANS equations. The standard k-ε turbulence model of Launder and Spalding [11] is employed to model the Reynolds stresses. This model solves two transport equations (for the turbulent kinetic energy, k, and its dissipation rate, ε) to calculate the eddy viscosity, μ_T. The model also involves five empirical model constants: $C_{\varepsilon1}$, $C_{\varepsilon2}$, C_μ, σ_k and σ_ε. Unless specified, we use the original model constants recommended by Launder and Spalding [11]. We also use wall functions to model the flow near the bottom of the channel, since here we consider a very high-Reynolds-number open-channel flow and it is impractical to resolve the viscous sublayer on the bottom wall. (Also, the k-ε model is a high-Reynolds-number model and cannot be applied to the viscous sublayer directly.)

As noted earlier, the turbines are modelled as porous discs, i.e. the effect of each turbine on the flow is modelled as a loss of momentum in the streamwise direction. Specifically, the loss of momentum (per unit area) is locally calculated as

$$M_z = K\left(\frac{1}{2}\rho U_d^2\right) \tag{9}$$

where K is the resistance coefficient of the discs (constant for all discs but varied for different cases simulated, see Table 1) and U_d is the local streamwise velocity at the disc plane. The thrust acting on each disc can therefore be calculated as

$$T_{d(i)} = \int_{disk(i)} M_z \mathrm{d}A = \frac{K}{2}\rho\left\langle U_d^2\right\rangle_i A_d \tag{10}$$

where the integration is taken over the area of each disc, A_d (= $\pi d^2/4$), the subscript "i" indicates the i-th disc in the array of n discs (n = $8n_R$), and $\langle\varphi\rangle_i$ denotes the average of a variable φ over the i-th disc surface. Hence the (global) thrust coefficient averaged across all n discs is

$$C_{TG} = \frac{\sum_{i=1}^{n} T_{d(i)}}{\frac{1}{2}\rho u_{d0}^2 n A_d} = K\frac{\left\langle U_d^2\right\rangle}{u_{d0}^2} \tag{11}$$

where $\langle\varphi\rangle$ denotes the average of φ over all n discs and u_{d0} (= 2.05m/s) is the velocity averaged across the disc area for the "undisturbed" case (K = 0). Also, the power removed from the flow by the i-th disc is

$$P_{d(i)} = \int_{disk(i)} M_z U_d \mathrm{d}A = \frac{K}{2}\rho\left\langle U_d^3\right\rangle_i A_d \tag{12}$$

and hence the (global) power coefficient averaged across all n discs is

$$C_{PG} = \frac{\sum_{i=1}^{n} P_{d(i)}}{\frac{1}{2}\rho u_{d0}^3 n A_d} = K\frac{\left\langle U_d^3\right\rangle}{u_{d0}^3} \tag{13}$$

Also, the (global) axial induction factor averaged across all n discs is

$$a_G = 1 - \frac{\langle U_d\rangle}{u_{d0}} \tag{14}$$

As shown in [12] this RANS porous disc model agrees well with the analytical single-scale blockage model of Garrett and Cummins [2] if applied to a single disc located in the middle of a rectangular channel with low ambient turbulence; see [6] and [12] for further details.

C. Computational grids

The computational grids for this study were created using ANSYS ICEM CFD. A special care was taken to make sure that the total number of grid points used for each grid was less than 2 million to save computational costs, since a number of cases (76 cases shown in Table 1 and some additional cases) were required to study this problem systematically.

To create grids for several different array configurations quickly and systematically, we first created a 2D unstructured mesh for a cross section of the channel and then extruded it along the streamwise direction. Figure 1 shows part of the 2D cross-sectional mesh. In order to ensure a good enough mesh quality, the 2D cross section was divided into 4 regions: disc (maroon), near-disc (purple), far-disc (green) and near-wall (pink) regions. For the near-wall region, we used a structured mesh with clustering grid points in the vicinity of the wall, resulting in reasonably small wall y^+ values of less than 100 for the entire bottom wall.

The 2D cross-sectional mesh was then extruded along the streamwise direction to create the final 3D mesh for the entire channel. Figure 2 shows an isometric view of roughly half of the 3D mesh for a single row case. 160 grid points were used

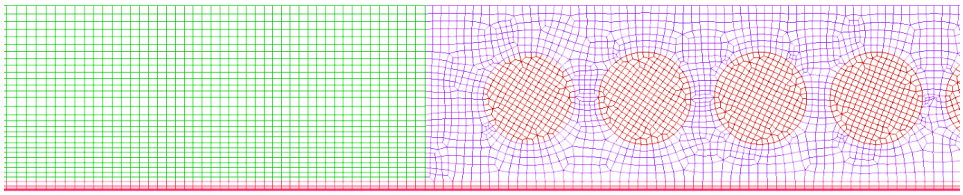

Fig. 1 Partial view of the cross-sectional mesh.

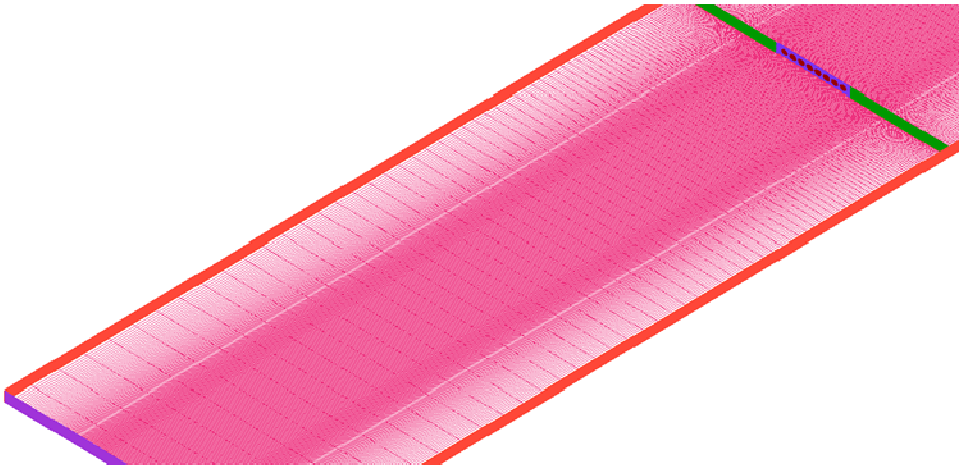

Fig. 2 Isometric view of the 3D channel mesh for a single row case.

for the channel length (80 points for upstream and another 80 points for downstream of the discs) with the smallest spacing of 1m (0.05d) near the discs and the largest spacing of 25m (1.25d) far upstream and far downstream of the discs. The use of such high aspect ratio elements (to reduce the total number of grid points) is justified since the (Reynolds-averaged) flow field far upstream and far downstream of the discs varies only very gently in the streamwise direction.

D. Boundary Conditions

A uniform streamwise velocity u = 2m/s was applied at the inlet boundary (100d upstream of the discs) together with k = 5.40×10^{-3} m^2/s^2 and ε = 6.52×10^{-6} m^2/s^3 (corresponding to a turbulent intensity of 3% and length scale of 10m). The inlet boundary was located far away from the discs so that the flow developed sufficiently before reaching the discs. For the top and side boundaries we used symmetry boundary conditions, whereas for the bottom (seabed) boundary no-slip conditions were applied (together with wall functions), creating vertically sheared flow around the discs. The disc surfaces were defined as internal boundaries with various resistance constant values to account for the momentum losses (Eq. (9)). For the outlet boundary, the streamwise gradients of all velocity components, k and ε were assumed to be zero.

E. Numerical Schemes

All simulations were performed using ANSYS FLUENT, which is based on the finite volume method. The simulations were performed as steady state, using the SIMPLE algorithm for velocity-pressure coupling [13]. For spatial discretization, second-order upwind schemes were used for the momentum, k and ε. Each simulation was run long enough to make sure that the results (especially a_G, C_{TG} and C_{PG}) were fully converged; see [14] for further details.

IV. Results and Discussion

A. Single Row Cases

Figure 3 shows the (global) thrust and power coefficients, C_{TG} and C_{PG}, obtained from the RANS simulations (symbols) and the two-scale ADT (lines) for four different disc-spacing cases: s/d = 0.25, 0.5, 1 and 4. It can be seen that the RANS results agree qualitatively with the two-scale ADT, i.e. both predict the same trend in terms of the effects of disc-spacing on the variations of C_{TG} and C_{PG}. The highest power extracted by these 8 discs is obtained for the smallest disc-spacing case (s/d = 0.25) and the power decreases as the spacing increases. Also, the (global) axial induction factor required to maximise the power decreases as the spacing increases.

Although the trends of these results agree between the two-scale ADT and RANS simulations, the values of C_{PG} (and also C_{TG}) do not agree quantitatively. For the cases with relatively small disc-spacing (s/d = 0.25, 0.5 and 1) the RANS results are lower than the theory (presumably because the relatively small number of discs arrayed [6]), whilst for the case with a large disc-spacing (s/d = 4) the RANS results are higher than the theory (presumably due to the effect of near-wake mixing neglected in the theory [12]).

Figure 4 shows streamwise velocity contours plotted on the "hub-height" plane (y = 0) for the two smallest disc-spacing cases (s/d = 0.25 and 0.5). The resistance coefficient K = 4.5 is very close to the optimal value. Note that the flow direction

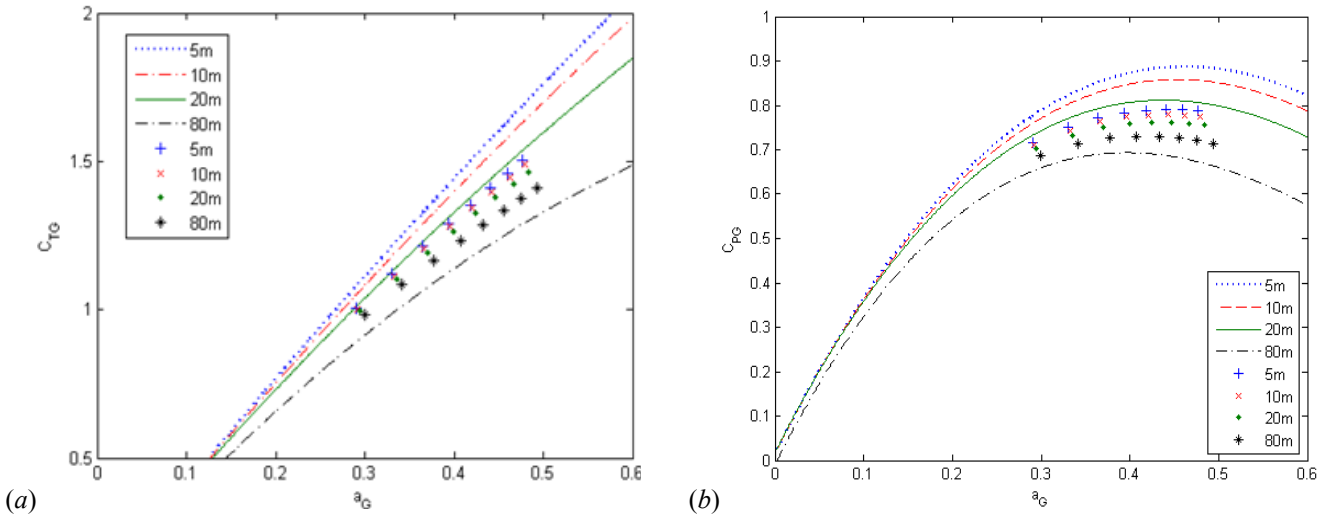

Fig. 3 Comparison of the two-scale ADT and RANS simulations for a single row of turbines: (*a*) thrust coefficient C_{TG} vs. axial induction factor a_G; and (*b*) power coefficient C_{PG} vs. axial induction factor a_G. Lines and symbols show the results of two-scale ADT and RANS simulations, respectively.

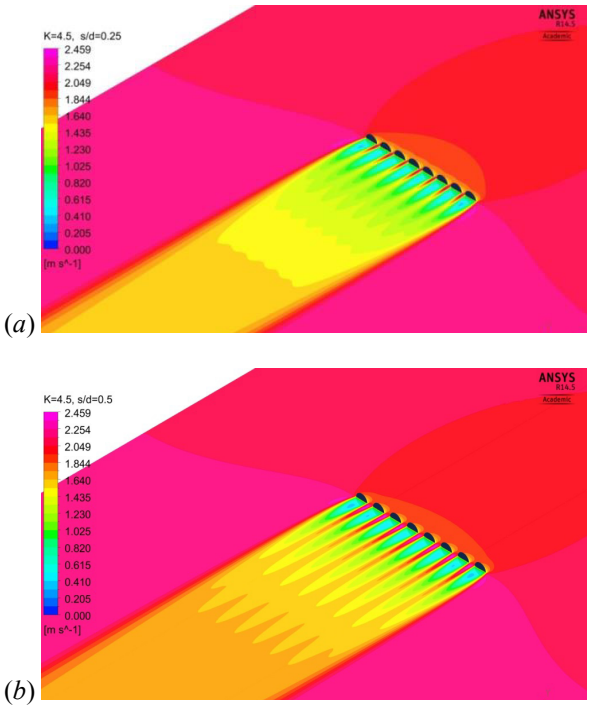

Fig. 4 Streamwise velocity contours plotted on the hub-height plane: (*a*) $s/d = 0.25$, $K = 4.5$, $a_G = 0.44$; (*b*) $s/d = 0.5$, $K = 4.5$, $a_G = 0.44$.

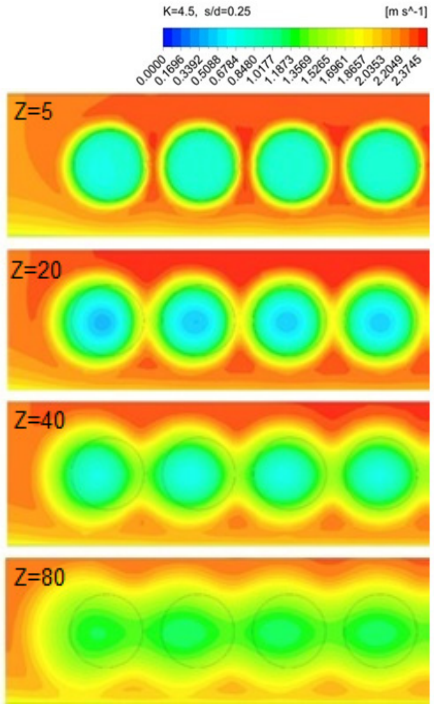

Fig. 5 Streamwise velocity contours plotted at 0.25*d*, 1*d*, 2*d* and 4*d* downstream of a single row of 8 discs ($s/d = 0.25$, $K = 4.5$).

is from upper right to lower left. It can be seen that, although the number of discs arrayed is relatively small, the expansion and mixing of the flow take place at two dominant scales, i.e. device scale and array scale. The array-scale flow deceleration occurs first upstream of the entire array (red to dark orange in the figure) and then the device-scale flow deceleration occurs just upstream of each disc individually (dark orange to light orange). Also, the device-scale mixing takes place much faster behind each disc compared to the array-scale mixing behind the entire array. The device-scale wake mixing can be seen in more detail in Figure 5, which shows the streamwise velocity contours at four different streamwise locations (0.25*d*, 1*d*, 2*d*, and 4*d* downstream of the discs) for the case with $s/d = 0.25$. These two-scale flow features are similar to those observed in the earlier RANS study [6] that neglected the vertical shear.

B. Double Row Cases

Figure 6 compares C_{PG} for the double row cases obtained from the RANS simulations (symbols) and the two-scale ADT (lines). The results shown here are for $s/d = 0.25$, 0.5 and 1.

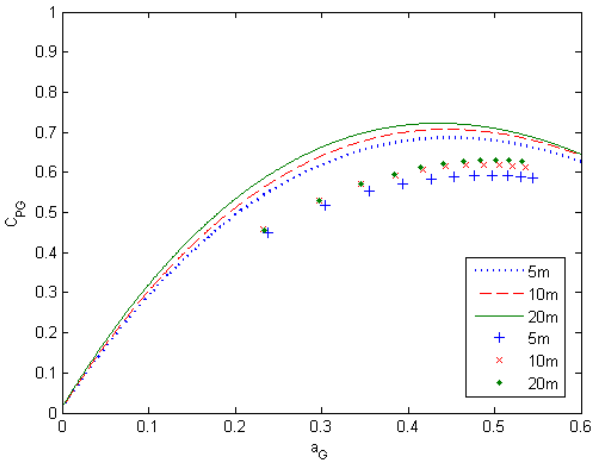

Fig. 6 C_{PG} vs. a_G for double rows of turbines. Lines and symbols show the results of two-scale ADT and RANS simulations, respectively.

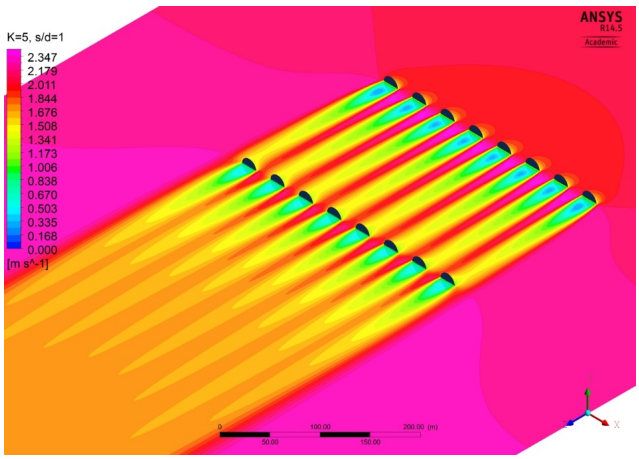

Fig. 7 Streamwise velocity contours plotted on the hub-height plane (double-row case, $s/d = 1$, $K = 5$, $a_G = 0.50$).

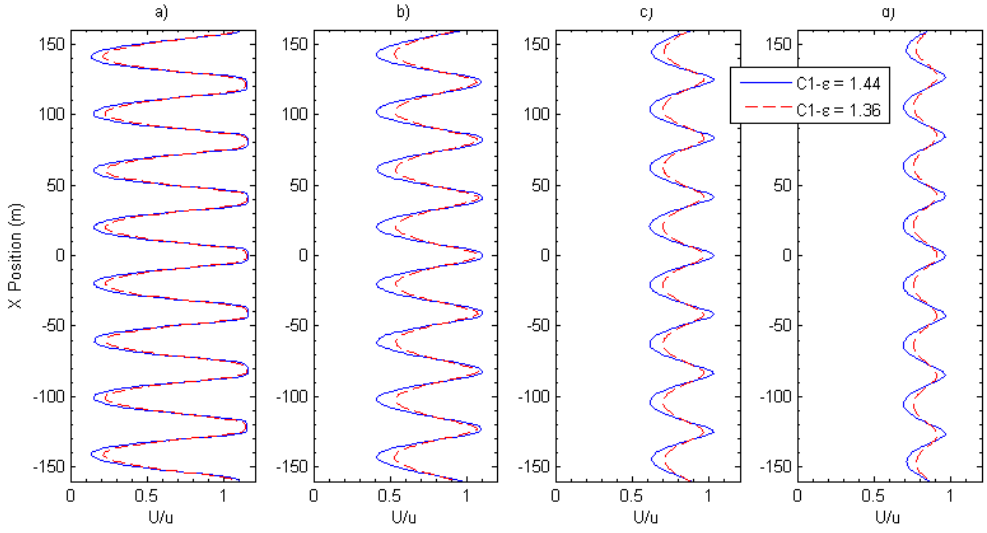

Fig. 8 Streamwise velocity profiles downstream of the front row of turbines at the hub height (double-row case, $s/d = 1$, $K = 5$): (*a*) 1*d* downstream; (*b*) 2.5*d* downstream; (*c*) 5*d* downstream; and (*d*) 7.5*d* downstream. $C_{1\varepsilon} = 1.44$ and 1.36 represent standard and stronger wake mixing cases, respectively.

As noted earlier, the streamwise gap between the two rows is fixed at 10*d* for all cases. Again, the RANS results agree qualitatively with the two-scale ADT and importantly, both predict the same trend in terms of the effect of disc-spacing. Here the highest power is obtained for $s/d = 1$ (s = 20m) and the power decreases as the spacing is reduced, suggesting that the optimal local blockage ratio for double rows of turbines is much lower than that for a single row of turbines. Note that the same conclusion has been obtained recently by Draper and Nishino [10], who employed a different two-scale approach as described earlier in Section II.B.

Although the results agree qualitatively, the discrepancies in C_{PG} are larger for the double row cases than for the single row cases. The values of C_{PG} predicted by the present RANS simulations are much smaller than the two-scale ADT. This is presumably mainly because the streamwise spacing between the rows is not large enough to neglect the device-scale wake interaction in the present RANS simulations. Figure 7 shows streamwise velocity contours plotted on the hub-height plane for the highest power case ($s/d = 1$, $K = 5$). It can be seen that the wake of each disc in the upstream row has not been fully mixed before reaching the downstream row. It should also be noted, however, that discs at the ends of the downstream row are not completely covered by the wake of the upstream discs because the wake of the entire upstream row has already been expanding slightly in the spanwise direction before reaching the downstream row (i.e. disc wakes near the spanwise ends of the rows are somewhat "staggered" even though the discs are perfectly aligned and not staggered geometrically).

To understand the effects of device-scale wake mixing on the performance of double rows of turbines, some additional cases with stronger wake mixing were simulated by changing one of the turbulence model constants, $C_{\varepsilon 1}$, from the original value of 1.44 to a slightly smaller value of 1.36 (see [6] for a justification of this approach). Figure 8 shows the streamwise velocity profiles at 1*d*, 2.5*d*, 5*d* and 7.5*d* downstream of the

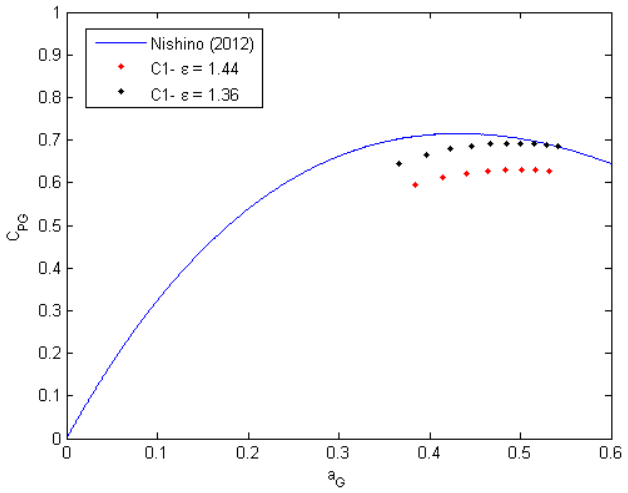

Fig. 9 C_{PG} vs. a_G for double rows of turbines with s/d = 1. Line and symbols show the results of two-scale ADT and RANS simulations, respectively.

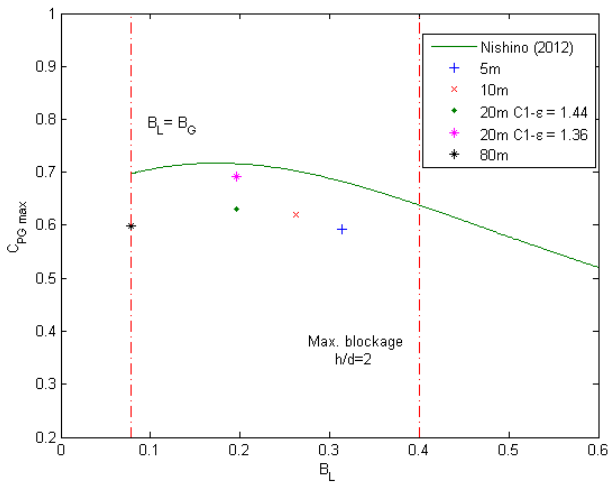

Fig. 10 The maximum power coefficient ($C_{PG\,\max}$) vs. local blockage ratio B_L for double rows of turbines. Green line shows the two-scale ADT and symbols show the results of RANS simulations. Note that the red dash-dot lines indicate the possible range of B_L by definition.

front row of discs for the standard ($C_{\varepsilon 1}$ = 1.44) and stronger ($C_{\varepsilon 1}$ = 1.36) wake mixing cases. As expected, the wake behind each disc is mixed faster for the case with $C_{\varepsilon 1}$ = 1.36. It can also be seen that the wake of the entire front row is expanding slightly in the spanwise (x) direction and that the difference in $C_{\varepsilon 1}$ does not affect this spanwise expansion of the array-scale wake. Hence we can analyse the effects of the strength/rate of device-wake mixing by comparing these two cases.

Figure 9 compares the (global) power coefficient values for these two different wake mixing cases together with the two-scale ADT. It can be seen that the stronger wake mixing case ($C_{\varepsilon 1}$ = 1.36) predicts higher C_{PG} values which are much closer to the two-scale ADT. This is presumably because the device-scale wake interaction between the two rows is less significant for the stronger mixing case. It should be noted, however, that the value of a_G required to achieve the highest power is still somewhat different from the theory. To understand better the reasons of these discrepancies, we would need further studies with a larger number of discs arrayed in each row.

Finally, Fig. 10 compares the maximum values (for a given local blockage ratio) of the (global) power coefficient, $C_{PG\max}$, obtained from the two-scale ADT and the RANS simulations. Note that the two vertical lines indicate the possible range of the local blockage ratio for the present study; the smallest B_L corresponds to the largest possible intra-disc spacing (s/d = 4) and the largest B_L corresponds to the smallest possible spacing (s/d = 0). It can be seen that the theory agrees reasonably well with the simulations in terms of the prediction of the optimal local blockage ratio, which is around 0.2 for this double-row case, despite the fact that the assumptions (regarding the scale separation and negligible device-wake interaction) used in the theory are not fully satisfied in this case.

V. Concluding Remarks

In this study we have performed 3D RANS simulations of single and double rows of 8 porous discs placed in the middle of a wide channel with a vertically sheared flow, with the aim of numerically validating the two-scale ADT. We summarised the theory for a single row of turbines first and then explained a possible extension of the theory to double (and more) rows of turbines. For the double (and more) rows of turbines, the main assumption for the theory to be valid is that the stream-wise spacing between each row is large enough to neglect the device-scale wake interaction between the rows, i.e. the wake behind each turbine (not the entire row) is fully mixed before reaching the downstream turbines. It has also been explained that there are two possible approaches to the array-scale part of the two-scale ADT for multiple rows of turbines and, for the approach used in this study, the number of turbines (within each row) required to satisfy the scale-separation assumption will increase with the number of rows.

For the single row of 8 porous discs, our RANS simulation results agreed qualitatively with the two-scale ADT in terms of the effect of intra-disc spacing on the total power predicted. Both RANS and two-scale ADT predicted the highest power with the smallest disc-spacing tested (s/d = 0.25), even though the power coefficient values obtained from the RANS did not agree quantitatively with the theory (presumably because the number of discs arrayed was relatively small). The two-scale flow features observed in our RANS results were also similar to those observed in the earlier study [6] that neglected the vertical shear of the flow. Therefore it seems that, at least for this size of array consisting of 8 devices, neglecting the effect of seabed friction (and the induced vertical shear of the flow) is indeed a good first-order approximation for predicting the performance of the array theoretically.

For the double rows of 8 porous discs, again our simulation results agreed qualitatively with the two-scale ADT in terms of the effect of intra-disc spacing. Both predicted the highest total power with a relatively small local blockage ratio B_L of about 0.2 (corresponding roughly to s/d = 1) for this case. However, agreement in the power coefficient values predicted was worse compared to the single row case. This discrepancy

was mainly due to the small streamwise spacing between the two rows (10d) used in this study, causing substantial device-scale wake interaction between the rows. Some corrections to the theory would therefore be needed to predict quantitatively the performance of such double rows of turbines with a small spacing between each row. A potential difficulty in modelling this device-scale wake interaction is that turbines downstream may or may not be within the wake of the turbines upstream, depending on how much the wake of the entire upstream row expands laterally before reaching the downstream row. This means that device-scale wakes can be effectively "staggered" (i.e. shifted slightly in the lateral direction) even if the devices themselves are not arrayed in a staggered manner.

Finally, it should be noted that the two-scale ADT has not been validated for real turbines; all relevant studies reported so far (including the present study) are for ideal actuator discs or porous discs. The theory should therefore be compared with real turbine experiments and/or computations in future studies in order to assess, for example, the influence of the rotation of individual turbine wakes on the characteristics of array-scale wakes. Also of importance but not examined in this study is the validity of using an actuator disc model in a sheared flow, which has been investigated very recently for the single-scale ADT [15] but not for the two-scale ADT. Nevertheless, it is encouraging that the RANS simulations of porous discs in a vertically sheared flow predicted the same optimal intra-disc spacing as the theory, not only for the single-row case but also for the double-row case. Further validations and modifications of the theory will be necessary in future studies, especially on: (i) how to apply the theory to real turbines; and (ii) how to incorporate the device-scale wake interaction into the theory (for multi-row cases).

REFERENCES

[1] A. Betz, *Introduction to the Theory of Flow Machines,* Oxford, UK: Pergamon Press, 1966.

[2] C. Garrett and P. Cummins, "The efficiency of a turbine in a tidal channel," *J. Fluid Mech.*, vol. 588, pp. 243–251, Oct. 2007.

[3] G. T. Houlsby, S. Draper, and M. L. G. Oldfield, "Application of linear momentum actuator disc theory to open channel flow," Dept. of Eng. Sci., Univ. of Oxford, Oxford, UK, Tech. Rep. OUEL 2296/08, 2008.

[4] J. I. Whelan, J. M. R. Graham, and J. Peiró, "A free-surface and blockage correction for tidal turbines," *J. Fluid Mech.*, vol. 624, pp. 281–291, 2009.

[5] T. Nishino and R. H. J. Willden, "The efficiency of an array of tidal turbines partially blocking a wide channel," *J. Fluid Mech.*, vol. 708, pp. 596–606, Oct. 2012.

[6] T. Nishino and R. H. J. Willden, "Two-scale dynamics of flow past a partial cross-stream array of tidal turbines," *J. Fluid Mech.*, vol. 730, pp. 220–244, Sep. 2013.

[7] T. Nishino and S. Draper, "Local blockage effect for wind turbines," *J. Phys.: Conf. Ser.*, Vol. 625, 012010, Jun. 2015.

[8] T. A. A. Adcock, S. Draper, and T. Nishino, "Tidal power generation – a review of hydrodynamic modelling," *Proc. IMechE, Part A: J. Power and Energy* (in press).

[9] T. Nishino, "Research Memorandum," Tidal Energy Research Group, Univ. of Oxford, UK, 13th April 2012.

[10] S. Draper and T. Nishino, "Centred and staggered arrangements of tidal turbines," *J. Fluid Mech.*, vol. 739, pp. 72–93, Jan. 2014.

[11] B. E. Launder and D. B. Spalding, "The numerical computation of turbulent flows," *Comput. Methods Appl. Mech. Eng.*, vol. 3, pp. 269–289, 1974.

[12] T. Nishino and R. H. J. Willden, "Effects of 3-D channel blockage and turbulent wake mixing on the limit of power extraction by tidal turbines," *Int. J. Heat Fluid Flow*, vol. 37, pp. 123–135, 2012.

[13] S. V. Patankar, *Numerical Heat Transfer and Fluid Flow*, Washington D. C., USA: Hemisphere Publishing Corporation, 1980.

[14] E. Perez-Campos, "CFD analysis for optimal single and double rows of marine turbines in a wide channel," M.Sc. thesis, Cranfield University, Cranfield, UK, 2014.

[15] S. Draper, T. Nishino and T. Adcock, "Turbine blockage in non-uniform flow," *Proc. 19th Australian Fluid Mechanics Conference*, Melbourne, Australia, Dec. 2014.

Numerical validation of the two-scale actuator disc theory for marine turbine arrays

Perez-Campos, Edgar

2015-09-11

Edgar Perez-Campos and Takafumi Nishino. Numerical validation of the two-scale actuator disc theory for marine turbine arrays. Proceedings of the 11th European Wave and Tidal Energy Conference, 6-11 September 2015, Nantes, France.

http://dspace.lib.cranfield.ac.uk/handle/1826/10608